

Persistent Deformation in a Post-Collisional Stable Continental Region: Insights from 20 Years of cGPS in Romania

Alexandra Muntean^{1*}, Laura Petrescu^{1,2} Boudewijn Ambrosius³, Felix Borleanu¹, Eduard Ilie Nastase¹, Ioan Munteanu^{4,5}

¹National Institute for Earth Physics, Măgurele, 077125, Romania

²Faculty of Physics, University of Bucharest, Măgurele, 077125, Romania

³Faculty of Aerospace Engineering, Delft University of Technology, Delft, 2629HS, The Netherlands

⁴Faculty of Geology and Geophysics, University of Bucharest, Bucharest, 010041, Romania

⁵Romanian Academy Institute for Geodynamics “Sabba Stefanescu”, Bucharest, 020032, Romania

Correspondence to: Alexandra Muntean (muntean@infp.ro), Laura Petrescu (laura.petrescu@infp.ro), Boudewijn Ambrosius (bacambrosius@gmail.com).

Abstract. The Carpathian Region, located at the edge of the East European Platform, presents a unique tectonic setting where major deformation associated with subduction and collision appears to have ceased around 8 million years ago. Yet vertical movements and seismicity continued afterward till the present day, suggesting ongoing crustal deformation and challenging our understanding of intraplate earthquakes and the processes driving these phenomena in an area considered a stable continental interior. In this study, we analyze over two decades of continuous GPS (cGPS) data from 143 permanent stations to estimate both horizontal and vertical crustal motions, constructing the most accurate model of crustal deformation in the region to date. The estimated velocity field indicates a southward drift of the South Carpathians and Moesia relative to Eurasia, with velocities ranging from 0.5 to 2 mm/yr. We detect a more complex pattern of vertical uplift and subsidence in the foredeep, challenging a previously held view that this region is solely subsiding. This pattern may reflect localized uplift in response to processes such as the Vrancea Slab break-off beneath the South-East Carpathians. Crustal-scale active faults accommodate the observed differential motion, fragmenting the foreland. Furthermore, using a regularized horizontal velocity vector field, we estimate strain rate variations, maximum shear strain, and dilatation patterns across Romania, which align with observed stress regimes and earthquake mechanisms. This agreement validates our results and indicates an influence of surface plate kinematics on the observed seismicity, in addition to the deep Vrancea Slab dynamics. Our findings provide insights into the causes of crustal deformation at the transition between active collision zones and stable continental platforms, enhancing our understanding of intraplate seismicity in regions traditionally considered tectonically stable.

Keywords: deformation, GPS, crustal motion, geology, tectonics.

1. Introduction

A key tectonic question lies in understanding the nature of active deformation and frequent seismicity in regions situated at the transition between subduction/collision systems and more stable continental interiors. The Carpathian Region in Romania marks such a transition between the active Africa-Eurasia subduction system to the south and the stable continental core of Eurasia: the East European Platform (Fig. 1). Although this area is not

37 considered a traditionally active plate boundary, with most geological evidence suggesting that major deformation
38 associated with the collision ceased around 8 million years ago (Mațenco and Bertotti, 2000), it continues to
39 experience frequent crustal and subcrustal seismicity. Active deformation and seismicity are observed along major
40 faults and geological contacts (e.g., swarms near Tg. Jiu and Galați, Craiu et al., 2017; Radulian et al., 2023;
41 Borleanu et al., 2024). Notably, the Vrancea Slab, a relic lithospheric plate sinking, retreating, and stretching
42 beneath the East Carpathians Bend Zone, may still be coupled with the overlying crust, as suggested by the
43 thermochronological studies, which showed an increase in uplift, post 8 Ma, especially along the western flank of
44 the Focsani Basin (Necea et al., 2005, 2013, 2021). This coupling could be driving long-term surface deformation
45 (Ismail-Zadeh, 2012; Petrescu et al., 2021), contributing to ongoing seismicity (Radulian et al., 2019; Petrescu et
46 al., 2025) and exhibiting the largest present-day strain concentration in continental Europe (Wenzel et al., 1999).

47 Measuring crustal motion is relevant for understanding ongoing deformation processes and seismic hazards in
48 such a tectonically complex region. In this study, we estimate both horizontal and vertical motions using Global
49 Positioning System (GPS) data from permanent stations that operated in Romania in the past 20 years. These
50 measurements provide key information about how the region is deforming and how this relates to the observed
51 seismicity. The data also shed light on the connection between surface deformation and subsurface dynamics,
52 including the potential role of the sinking slab in driving seismic activity. Furthermore, the GPS data allows us to
53 assess whether deformation is concentrated along major fault zones or more broadly distributed across the crust,
54 offering a clearer picture of how past tectonic events continue to shape the region's seismic behavior.

55 The first vertical velocity maps of Romania, based on repeated leveling data from first- and second-order national
56 network lines, were published by Cornea et al. 1978, 1979a, 1979b. Following the major earthquake of March 4,
57 1977 (M7.2), high-accuracy leveling measurements allowed for the development of a more refined vertical
58 velocity map (Popescu and Drăgoescu, 1987). Subsequent research extended these efforts to the broader Carpatho-
59 Balkan region (Joó et al., 1987). Dinter and Schmitt (2001), after two years of GPS monitoring in Romania,
60 detected no measurable deformation but recommended expanding the network and conducting repeated
61 measurements at two-year intervals to capture crustal dynamics better. Van der Hoeven et al. (2005) later
62 published results from annual GPS campaigns conducted between 1997 and 2004. However, velocity solutions
63 derived from temporary GPS deployments were subject to influences such as equipment changes, monument
64 removals, and antenna setup inconsistencies, as well as local effects such as sediment compaction and site
65 instability. Compared to the high precision of modern continuous GPS (cGPS) solutions, the historical campaign
66 data exhibit three to four times higher uncertainty (van der Hoeven et al., 2005). These limitations highlight the
67 need for continuous GPS measurements to better resolve crustal and mantle dynamics in geologically active
68 regions.

69 **2. Tectonic setting**

70 The tectonic evolution of the Romanian region is essential for understanding present-day deformation and seismic
71 activity. The Carpathian Mountains dominate the topography, with neo-tectonic and associated seismicity
72 pervasive in the East Carpathians Bend Zone and extending into the South Carpathians and the surrounding
73 foreland (Petrescu et al., 2021), underlain by the Moesian Platform (MP), a thick lithospheric block with

74 Precambrian-aged basement, shaped by multiple tectonic phases throughout the Paleozoic to Cenozoic times (Fig.
75 1). Th MP is bounded by two Alpine Orogens, the Carpathians to the north and West and the Balkanides to the
76 south, while the eastern margin extends into the Black Sea Basin. It is largely covered by Neogene sediments and
77 extends eastward to the Black Sea, where its uplifted basement is exposed in the Dobrogea Region. The platform
78 is separated into crust blocks by several faults, such as the Intra-Moesian Fault (IMF) and the Capidava-Ovidiu
79 Fault (COF, Fig. 1).

80 To the northeast, the MP transitions into the East European Platform (EEP), a thick and geologically stable
81 continental core that forms part of the Eurasian Plate. The boundary between the two is marked by the North
82 Dobrogea Orogen (NDO) (Hippolyte, 2002), a remnant of the Hercynian Orogeny (Seghedi et al., 1999), located
83 between the Peceneaga-Camena Fault (PCF) and Sfântul Gheorghe Fault (SGF, Fig. 1). Part of this now partially
84 eroded orogen is buried beneath Neogene foredeep sediments from the younger Carpathian collision, while to the
85 east, it has undergone uplift.

86 Over the past 20 million years, the concomitant roll-back of the Carpathian and Dinaridic Slab Adria Plate led to
87 the opening of the Pannonian Basin coeval with the formation of the Carpathian Fold and Thrust Belt of the Outer
88 Carpathians and associated foreland basin (Balla, 1986; Barrier et al., 2018; Maţenco and Radivojevic, 2012),
89 essentially shaping the present-day European continent (Schmid et al., 2020). In Romania, the slab roll-back
90 forced the clock wise rotation of the Carpathian Orogen and obliquely thrusting over the foreland units MP,
91 forming the South Carpathians, and collided with the passive margin of the East European Platform, creating an
92 asymmetric foreland basin (Săndulescu, 1984; Maţenco and Bertotti, 2000; Csontos and Vörös, 2004).

93 Beneath the Southeast Carpathians, where multiple tectonic units interact, the notorious Vrancea Slab, a
94 lithospheric block that is plunging almost vertically into the mantle (Ren et al., 2012). It is stretching and causing
95 frequent high-magnitude destructive earthquakes in Romania, both at intermediate depths and in the overlying
96 crust (Radulian et al., 2019; Petrescu et al., 2021; Enescu et al., 2023). Analysing the crustal motions above this
97 sinking slab provides an opportunity to gain insights into crustal deformation in a triple-junction tectonic setting
98 (Beşuţiu et al., 2017). Major collisional-related shortening deformation in the Carpathians is thought to have ended
99 around 8-11 Ma, based on the cessation of late Miocene thrusting (Maţenco et al., 2007 and references therein),
100 while fission-track analysis suggests the onset of exhumation (or uplift) at 4 Ma in the SE Carpathians and 12 Ma
101 in the East and South Carpathians (Sanders et al., 1999; Cloetingh et al., 2006). Present-day GPS measurements
102 provide valuable insights into how these long-term geological processes continue to shape ongoing crustal motion
103 and deformation, particularly in the Vrancea Zone (Fig. 1), where slab-related dynamics are still influencing
104 surface motion. The crustal deformations observed today are also influenced by the relative motion of surrounding
105 crustal blocks, complicating the understanding of the region's complex and dynamic geological behavior.

106 **3. Continuous GPS (cGPS) Networks in Romania**

107 We analyzed data from cGPS stations across Romania, which are part of four different networks (Fig. 1). The
108 primary network, supported by the National Institute for Earth Physics (NIEP), was first developed in 2001.
109 Initially, the network consisted of seven stations, equipped with Leica CRS1000 receivers and LEIAT504 choke-
110 ring antenna protected by a dome. These stations were placed in remote areas and were designed to operate with

111 minimal maintenance, relying on power converters and batteries. Over time, the network has grown, and today it
112 includes 33 stations, with five of the original stations still in use. The newer stations are equipped with Leica
113 GRX1200, LEIAR GR30, and GR50 receivers. Most of the antennas are Leica (LEIAT504, LEIAR10, LEIAR20)
114 and are placed on concrete pillars. Only one is mounted on a polar mast (MNG2). The stations transmit real-time
115 data via the internet, and NIEP is responsible for the equipment, installation, ongoing maintenance, and data
116 analysis.

117 We also used GPS data from the GeoPontica network, developed by the National Research and Development
118 Institute for Marine Geology and Geoecology (GeoEcoMar), the National Center for Monitoring and Alarm to
119 Natural Marine Hazards – Euxinus, covering the period from 2013 to the present. This network includes 13
120 stations, the antennas are mounted on a deep-drilled, braced monument. In addition, we included data from the
121 ROMPOS (NACLAR) network, managed by the National Agency for Cadastral and Land Registration, comprising
122 86 reference stations across Romania. We were also granted access to data from the private TopGeocart network,
123 which includes 8 stations. Most of these GPS antennas are mounted on building rooftops or fixed to the structures
124 housing the receivers.

125 In total, this selection resulted in 143 available stations. The data are stored in a repository, organized by network,
126 year, and Julian day, in the Receiver Independent Exchange (RINEX) version 2 and 3 format, sampled at 30s
127 intervals. For this study, we only selected stations that are (still) operational after January 01, 2024. This reduced
128 the selection to 130 stations (Fig.1).

129 **4. GPS data processing**

130 For the data processing, we use the GipsyX software (Bertiger et al., 2020), developed at NASA's Jet Propulsion
131 Laboratory (JPL), Pasadena, USA. It features Precise Point Positioning (PPP), which enables (daily) geodetic
132 position determination of a single GPS station. Accuracy can vary depending on the quality of the GPS receiver,
133 the antenna, and local conditions (e.g., multipath). Weekly updated data files, provided by JPL, contain precise
134 GPS satellite orbits, Earth Rotation Parameters (ERP), satellite clock corrections, spacecraft altitude information,
135 and so-called wide lane phase biases to enable signal ambiguity resolution. In addition, we apply ocean loading
136 corrections for each station, obtained from the Onsala Space Observatory, Chalmers University of Technology
137 (Bos and Scherneck, 2011). To model the wet tropospheric signal delays, we use data from VMF (Vienna Mapping
138 Functions) (re3data.org:VMF Data Server).

139 Processing the recordings from the 130 selected stations with this software resulted in a repository with daily
140 solutions for each station. Subsequently, to reduce noise, we combined the daily solutions into weekly ones. Then,
141 we converted the reference plate of these solutions to the Eurasian tectonic reference plate using the ITRF14
142 rotation parameters of that plate (Altamimi et al., 2017). From this data, we created a time series for each station.
143 To evaluate the impact of reference frame choice, we tested several local transformation approaches, including
144 Euler pole rotation, network mean removal, and selected-station mean removal. Statistical comparisons showed
145 that the Euler pole rotation was similar to the EU14 reference frame, which further justifies using EU14 as our
146 preferred reference frame (Figs. S1, S2, and S3; Tables S5 and S6 in the Supplementary Material - SM).

147 Next, we estimated a linear trend (velocity), yearly, and half-yearly seasonal signals. In addition, for
148 undocumented changes, the estimation model also includes position jumps at times identified from an inspection
149 of the raw time series. All recent time series are affected by a reference frame change on August 19, 2024, by
150 JPL. These are now also modeled as position jumps. An example of the results is presented in Figure 2 for the
151 long - lived station VRAP. Apparently, this station was re-equipped in 2011, and from the vertical residuals, it
152 seems that it took a few years to settle down on its original monument.

153 **4.1 Horizontal time series selection and quality control**

154 In this step, to ensure the best possible quality of the time series solutions, we selected stations with uncertainties
155 (sigmas) less than 0.2 mm/yr and velocity vectors smaller than 2 mm/yr. We consider that these criteria guarantee
156 a reliable selection of credible solutions. However, a small number of these sites still exhibit anomalous velocities.
157 These are likely caused by local effects such as landslides, station instability, local geological conditions,
158 subsurface compaction, undocumented antenna changes, and multipath interference. The main reason is that most
159 GPS antennas are mounted on buildings and unstable steel rods. In our analysis, we try to model them as position
160 jumps. The dates of these “unknown” jumps were established using a manual process by examining the “raw”
161 time series plots for each station.

162 This process automatically eliminates the shorter-lived time series, reducing the number of accepted solutions to
163 99, with the shortest series extending more than four years. This means that all 99 accepted solutions satisfy the
164 criterion established by Blewitt et al. (2001), who claim that the series should be longer than two and a half years
165 for a reliable estimate of the seasonal terms, which is essential for the reliability of the velocity estimate.

166 The accuracies (σ) at the 95% confidence level were estimated using the weighted root mean square (WRMS) of
167 the fit according to the formula:

$$168 \quad \sigma = \frac{2 \cdot WRMS}{2.4 \cdot T_{span}}$$

169 where T_{span} is the length of the time series in years. This approach provides estimates of velocities and their
170 uncertainties. This empirical approach relates the scatter of the residuals to the stability of the velocity estimate
171 and provides a practical measure of the combined effect of unmodeled noise sources. A similar approach has been
172 previously applied in geodetic studies (e.g., Muntean et al., 2016).

173 The use of WRMS-based uncertainties is justified by the relatively long duration of the analyzed time series (all
174 exceeding four years), which reduces the impact of temporally correlated noise on velocity estimation. In addition,
175 careful modelling of discontinuities (e.g., offsets due to equipment changes or local effects) further minimizes
176 bias in the residuals. Under these conditions, the adopted approach provides stable and internally consistent
177 uncertainty estimates across the network. Quantitatively, the mean uncertainty is 0.12 mm/yr, yielding a mean
178 signal-to-noise ratio of 4.9, with values reaching up to 15. These results indicate that the observed velocities
179 significantly exceed their formal uncertainties and are therefore well resolved (Fig. S4).

180 We also compared our results with those of Piña-Valdés (2022) for stations with common solutions and found an
181 average difference of less than 0.08 mm/yr (Fig. 3, and Figs. S4 and S5, SM). This level of agreement demonstrates
182 general consistency. The results for the 99 accepted sites are summarized in Table S1 in the SM.

183 **4.2 Creating a gridded, smooth horizontal velocity field**

184 To create a smooth, coherent representation of the computed time series solutions, we use a spatial gridding
185 approach: we set up an 8 x 8 grid of latitude and longitude nodes with each node linked to a square search box.
186 The size of these boxes depends on the distance (in km) between nearby nodes, ensuring the north-south and east-
187 west dimensions are equal. The next step we eliminate outliers with a velocity larger than two times the median.
188 Then, we calculate the average of the EW and NS velocity components of the remaining solutions. During this
189 process, 22 of the 99 solutions are excluded as outliers. The final result is a gridded dataset of 47 nodes showing
190 the velocities for each node. The other 17 nodes are not presented since there were no Romanian cGPS stations
191 available in the search area (see Table S2, SM).

192 When we include the literature (Piña-Valdés et al., 2022; Serpelloni et al., 2022), solutions for the countries
193 neighbouring Romania, the number of solutions increases to 160. After applying the aforementioned editing step,
194 this number decreases to 133. These solutions are based on a collection of shorter time series from before 2021.
195 Nevertheless, they provide valuable additional information.

196 **4.3 Vertical data selection**

197 For the vertical component, we apply a different approach. This component is hardly affected by horizontal station
198 instabilities, but mostly by undocumented antenna changes. We tackle this problem by estimating vertical position
199 jumps on the dates when they appear in the time series. Furthermore, we select only solutions with an absolute
200 velocity < 2 mm/yr and an accuracy < 1.0 mm/yr, which we consider credible. Some sites show subsidence, but
201 these are mostly located in coastal areas, on slow landslides, and compacting sedimentary areas. As a result, from
202 the 130 available solutions of the four Romanian permanent networks, 95 solutions were accepted (Fig. 4). The
203 results are presented in Figure 4 and Table S3 (SM). We also compared our solutions with those of Piña-Valdés
204 (2022) and found an average difference of less than 0.03 mm/yr.

205 When we include the literature solutions, the pattern does not change much. It mostly adds subsidence sites in the
206 area west and south-west of Romania. The total number of accepted vertical sites increased to 145.

207 **4.4 Strain rate estimation**

208 To better understand deformation and seismic hazard in this complex tectonic region, we further estimate strain
209 rate from the interpolated horizontal vector field of GPS velocities (Fig. 3). We use the open-source software
210 STRAINTOOL, which employs the VISR (Velocity Interpolation for Strain Rate) algorithm developed by Shen
211 et al. (2015). This algorithm interpolates our gridded solution to derive horizontal strain rates across the region,
212 using a weighted least squares approach on a denser regular grid. At each grid point, the horizontal velocity field
213 is approximated by a bilinear function, and a Gaussian function based on the distance between the interpolation
214 grid point and the other grid points is used for distance-weighting. This algorithm allows us to obtain the spatial
215 variation of strain rate, including the maximum shear strain rate (which indicates how much the crust is laterally

216 distorted), and the dilatational strain rate (which reflects areas of extension or compression). These are valuable
217 parameters for understanding the tectonic regime, whether a region is being compressed, extended, or sheared,
218 and how this deformation relates to observed earthquake focal mechanisms.

219 **5. Results**

220 **5.1 The horizontal velocity field**

221 Many horizontal velocity measurements indicate a predominantly southward movement in the MP, with variations
222 spanning approximately ± 20 degrees toward the southeast and southwest (Fig. 3). The IMF appears to mark a
223 slight orientation change from S-SE to S-SW oriented motion vectors. This shift is also reflected in the South
224 Carpathians, which are obliquely thrust over the MP, defined by strong and sometimes sharp lateral variation in
225 rheology across the major faults like IMF or COF, which imposed the formation of tear-faults and oblique ramps
226 into the Carpathian Orogen (Fig. 3). Hence, the magnitude and direction of motion vary significantly across the
227 IMF and COF or other major faults in the MP and foreland units in general, like PCF and NTF, that are defining
228 crustal blocks with different rheologies, thermal history, and response under the orogenic loading. In contrast,
229 vectors in the EEP show a slight northwestward motion relative to the Eurasian plate. This shift occurs across the
230 PCF and NTF, which define the boundaries of the North-Dobrogea Orogen (Fig. 3), a transitional zone between
231 the EEP margin and the MP. As a result, the EEP undergoes a subtle yet persistent movement relative to Eurasia,
232 diverging from the southward-moving MP through a series of crustal-scale faults that accommodate lateral
233 displacement.

234 The Transylvanian Basin (TB) and the East Carpathians, on the other hand, show minimal horizontal motion. GPS
235 stations in these areas indicate limited deformation, with inconsistent directional patterns and low overall
236 coherence in movement. Small horizontal motions are observed in the Pannonian Basin (PB) in an NNE direction,
237 which reoriented toward different directions near the Apuseni Mountains (see Figs. 1 and 3).

238 Overall, the foreland region, particularly the MP, appears to be drifting southward, while the other areas remain
239 relatively stable, indicating that the foreland is more dynamically active than the surrounding regions.

240 **5.2 The vertical velocity field**

241 The Carpathians predominantly experience uplift (Fig. 4), concentrated in the East Carpathians (e.g., BICA,
242 TPLT) and the South Carpathians (e.g., VAD2, and PITE). While some scattered stations (ROSU, TGTS) indicate
243 subsidence, the overall trend suggests uplift rates ranging between 0.5 and 2 mm/yr. The Vrancea bend zone is an
244 interesting exception because it only shows a minor uplift (e.g., LACP and VRAP).

245 The foreland region exhibits an intricate interplay of uplift and subsidence. The Moesian Platform, which occupies
246 the area bounded by the Carpathians, the Balkans, and the Black Sea, shows a north-south dichotomy in vertical
247 motion. In its southern part, across the E-W trending Danube River and towards the Balkans, the crust is
248 predominantly subsiding. Northward and northeastward toward the Carpathians, the Capidava-Ovidiu Fault, the
249 trend gradually transitions to uplift. The most pronounced uplift occurs in Dobrogea, the exposed basement of the
250 Moesian Platform near the Black Sea, where all geodetic stations record consistent uplift along the coast and the
251 Danube. Notably, the Danube changes its course northward across this transition zone.

252 The East European Platform, forming the eastern foreland of the Carpathians, exhibits only minor vertical
253 movements. Several stations in its northern part record slight uplift, which transitions southward into subsidence
254 toward the Neogene Troțuș Fault, known in literature as the New Troțuș Fault (Mațenco et al, 2007). This
255 subsiding trend extends farther south into parts of the NDO, continuing across the SGF and the PCF, which
256 delineates the boundary with the MP. On the opposite side, the MP is undergoing uplift, reflecting strong
257 differential crustal deformation along these seismically active fault networks.

258 In the back-arc region relative to the Carpathians, in the Transylvanian and Pannonian basins, estimated crustal
259 motions suggest subsidence relative to stable Eurasia. However, the Apuseni Mountains, a prominent highland
260 dividing the two subsiding basins, exhibit a cluster of stable and slightly uplifted motion vectors. Plotted vectors
261 range between -2 and +2 mm/yr, with an uncertainty of 1.0 mm/yr (Table S3 of the SM). This is a general feature
262 for most stations in Europe.

263 **5.3 GPS-estimated strain rates**

264 We estimated strain rate variation across Romania (Fig. 5) from the regularized horizontal velocity vector field,
265 and the distribution of maximum shear strain rate and dilatation (Figs. 6 a, b). The dilatation rate quantifies the
266 extent to which the Earth's crust is either expanding or contracting. It is derived by combining the principal strain
267 rates, with positive values indicating extension and negative values indicating contraction. High positive dilatation
268 values indicate regions experiencing extension, while negative values suggest compression, as seen in processes
269 such as thrust faulting. On the other hand, the maximum shear strain rate measures the degree of shear deformation
270 within the crust, without affecting its overall volume. This is determined by calculating the difference between
271 the principal strain rates. Elevated shear strain rates are associated with regions undergoing significant shear
272 deformation, such as strike-slip fault zones, while lower values typically occur in areas experiencing
273 predominantly extensional or compressional deformation.

274 The distribution of strain rates is quite complex (Fig. 5 and Table S4, SM), which is expected given the region's
275 complicated tectonic framework, with multiple blocks of diverse strengths converging to form a sinuous orogenic
276 track. The highest strain rates were estimated in the southwest, at the border between Romania and Serbia (Fig.
277 6a). This region also experiences the highest shear strain rate (Kr ezsek et al., 2013)

278 Dilatation patterns estimated from the strain tensor show a transition from compression in the PB to extension in
279 the intra-orogenic TB. The South Carpathians and the surrounding foreland regions, including the MP and the
280 EEP, are predominantly characterized by extension (Fig. 6b). However, localized areas of compression are
281 observed in the Eastern and South-East Carpathians, particularly in the Vrancea Zone.

282 **6. Discussion**

283 **6.1 Regional tectonic context**

284 To put our results in a broader context, we plot them against previous GPS-derived velocity vectors (Serpelloni
285 et al., 2022; Pi a-Vald es et al., 2022) in Figure 7. While there is some overlap with the Romanian networks, the
286 differences between datasets are minor. To reduce clutter in the figures and minimize the impact of large tectonic

287 motions in the south, we excluded stations with an absolute horizontal velocity exceeding 7 mm/yr, as shown in
288 Figure 7a, horizontal and 7b, vertical, with the UU-07 seismic tomography model of Amaru et al. (2007), updated
289 based on Wortel and Spakman (2000), at 200 km depth, serving as background.

290 In the regional plate tectonic context, the observed velocity field highlights the complex interactions between
291 major tectonic plates and blocks that converged in this geodynamically complex region. Seismic tomography
292 shows the high velocity thick cratonic lithosphere to the north-east which is supposed to be tectonically stable,
293 the Vrancea Slab as an elongated high velocity block sinking beneath the Carpathians, and the Adria and the
294 Hellenic slabs subducting beneath the Balkan Peninsula (Fig. 7). To the south, crustal motion velocities increase
295 significantly (Fig. 7), reflecting the rapid motion of the Hellenic subduction system as the African Plate subducts
296 beneath the Eurasian Plate, driving southeastward deformation in Greece. Eastward, the Anatolian Plate is moving
297 westward due to tectonic escape caused by the northward collision of the Arabian Plate with Eurasia. This
298 westward motion is a dominant feature of the eastern Mediterranean and plays a key role in accommodating the
299 overall regional deformation.

300 To the west, the Pannonian Basin, a hyper-extended lithosphere back-arc basin, shows relatively low horizontal
301 deformation rates, suggesting it is currently tectonically stable, with mirror positive inversion of its eastern margin.
302 However, the influence of the Adriatic Plate, a promontory of the African Plate, is meaningful. The Adria Plate,
303 subducting eastwards (Fig. 7), exerts a northeastward push on the Carpathian-Pannonian system, contributing to
304 compressional forces and tectonic inversion along the basin (Bada et al, 2007). These larger-scale processes
305 interact with the local tectonic architecture, such as the Vrancea Slab and associated seismicity (orange stars in
306 Fig. 7), resulting in a complex and heterogeneous deformation regime that bridges the stable cratonic lithosphere
307 and the active subduction-driven tectonics to the south and south-west.

308 **6.2 Correlation with earthquake mechanisms and stress indicators**

309 The GPS-derived strain rate field across Romania is characterized by a broadly distributed, long-wavelength
310 deformation pattern. At the regional scale, the field is dominated by N-S extension across much of the foreland
311 and the Carpathian chain, transitioning to localized E-W compression in the southwestern and eastern sectors (Fig.
312 6). While the GPS data provides a smooth representation of the velocity field, the discrete crustal deformation
313 captured by earthquake focal mechanisms (Fig. 5) and stress indicators from the World Stress Map (WSM2016,
314 Heidbach et al., 2007, Fig. 8) or from focal mechanisms inversion (Petrescu et al., 2021) offers a higher-resolution,
315 albeit more heterogeneous, view of how this regional strain is partitioned along inherited structures. This inherent
316 difference in spatial "wavelength" between geodetic and seismic data is essential for interpreting the transition
317 from plate-scale kinematics to fault-specific failure.

318 Despite these scale differences, we observe some spatial correlations between the strain rate and seismic regimes.
319 In the compressive domains, the negative dilatation rates observed in the Vrancea and the Eastern Carpathians
320 (Fig. 6b) align with clusters of thrust-faulting stress indicators (Fig. 8) and reverse-faulting mechanisms (Fig. 5),
321 confirming localized crustal shortening and compression at the bend zone. Conversely, the extensional signals
322 identified in the foreland and South Carpathians are corroborated by recent normal-faulting earthquake swarms,
323 such as those occurring near the SGF (Fig. 5 and Craiu et al., 2017) and recent intense seismic sequences in the
324 South Carpathians (Radulian et al., 2023; Borleanu et al., 2024). In areas characterized by high shear strain (Fig.

325 6a), specifically the southwestern Carpathians, the prevalence of strike-slip and oblique-slip focal mechanisms
326 (Fig. 5) reflects a complex regime of strain partitioning along major fault systems. This alignment across multiple
327 independent datasets, GPS, focal mechanisms, and stress indicators, supports the reliability of the derived strain
328 field.

329 In regions like the Moesian Platform, the relationship between geodetic strain and seismic indicators is more
330 nuanced. This variability in focal mechanisms, especially among smaller-magnitude events (M 3-4), likely
331 reflecting the activation of secondary, oblique faults accommodating local adjustments within the regional stress
332 framework. This complex pattern (Fig. 5) is particularly evident near large-offset faults where differing
333 rheological properties of crustal blocks that make up the MP (Mañenco et al., 2003; Petrescu et al., 2019) and the
334 influence of pre-existing lithospheric heterogeneities (e.g., Bertotti et al., 2003; Tărăpoancă et al., 2004) lead to
335 pronounced strain partitioning. While the smooth GPS field is not intended to resolve every local pocket of shear
336 or compression, the broad agreement between the primary strain axes and the dominant earthquake regimes
337 suggests that the geodetic model reflects the regional-scale deformation patterns characterizing the Romanian
338 crust.

339 **6.3 Interactions between slab dynamics and surface uplift**

340 Our results indicate a clear uplift trend in the foredeep basin area, supporting a typical post-collisional rebound
341 and uplift behavior, as observed in many other orogenic systems. These observations differ from previous
342 temporary GPS models (van der Hoeven et al., 2005) and lower resolution geological datasets (Merten et al., 2005,
343 2010), which suggested that subsidence dominated the evolution of the region as a typical response to slab
344 subduction and retreat (Tărăpoancă et al., 2004). This represents a notable change from earlier interpretations,
345 which tended to highlight uplift in the Dobrogea forebulge while assuming subsidence further towards the
346 Carpathian Orogen. This is also in line with some historical long-term repeated leveling methods (e.g., Popescu
347 and Drăgoescu, 1987; Joó et al., 1987) and is further supported by recent InSAR analyses (Poncoş et al., 2022).

348 The discrepancy may reflect either a shift in the tectonic regime over time or methodological limitations in
349 capturing ongoing geodynamic processes. The observed uplift may be associated with a partial decoupling
350 between the subducting lower lithosphere and the overlying crust (Petrescu et al., 2021), allowing stress relaxation
351 and isostatic rebound of the upper crust in the foreland. This scenario is consistent with the distribution of
352 intermediate-depth seismicity and the focal mechanism patterns observed in the Vrancea Zone. In addition,
353 Mitrofan et al. (2014) suggested a partial transmission of deformation from the slab to the crust, further supporting
354 the idea of vertical stress transfer from the mantle to the surface.

355 While the continued uplift in Dobrogea is confirmed, the GPS data suggest that this uplift extends into the
356 foredeep, highlighting the presence of vertical motions in the foredeep basin that are not solely driven by active
357 subduction dynamics. Instead, the observed uplift in both regions may be linked to slab break-off, a late-stage
358 process in the subduction and continental collision cycle (Andrews and Billen, 2009). As mentioned before, the
359 Dobrogea uplifted area at the transition to the Black Sea Basin is parallel to the SE Carpathians, again suggesting
360 the interplay between collisional processes affecting the Orogen and the flexural response of the lower plate, with
361 the forebulge outward migration (from the orogen), accompanied by coeval uplift and erosion.

362 Seismic imaging suggests that the Vrancea Slab has partially torn and rotated at ~150 km depth (Martin et al.,
363 2006), leaving a deeper slab segment (200-310 km) still weakly attached (Heidbach et al., 2007). If break-off
364 continues to be active (Müller et al., 2010), asthenospheric upwelling through the torn slab segment (Petrescu et
365 al., 2023) may be dynamically supporting present-day uplift in both the SE Carpathians and foredeep. Numerical
366 simulations of subduction-collision systems with spontaneous slab break-off (Duretz et al., 2011) predict post-
367 break-off uplift rates of 0.1-0.8 km/Myr (0.1-0.8 mm/yr), which closely match our observed uplift. Additionally,
368 an increase in slab dip may promote low-wavelength lithospheric folding following continental collision (e.g.,
369 Cloetingh et al., 2004; Mañenco et al., 2007), contributing further to the uplift observed in both the SE Carpathians
370 and the foredeep.

371 Our results also reveal a significant uplift in the East Carpathians (Fig. 4), not just the SE Carpathians, raising the
372 question of whether past slab break-off there (Nemcok et al. 1998) could still be influencing present-day vertical
373 motions. Geodynamic reconstructions suggest that the subducted passive margin of the East European Platform
374 progressively broke off from north to south along the East Carpathians (Sperner et al., 1996), culminating in the
375 currently detaching Vrancea Slab (Sperner et al., 2001; Koulakov et al., 2010; Lorinczi and Houseman, 2010).
376 While the initial isostatic response to slab break-off is expected to occur within a few million years (Duretz et al.,
377 2011) or up to 7 million years after convergence stops (Andrews and Billen, 2009), prolonged effects such as
378 mantle flow, residual buoyancy, and lower-crustal flow could be sustaining regional uplift. This interpretation is
379 further supported by Bouguer gravity anomalies (Fig. 8), which show relatively positive values (0–40 mGal) over
380 the mountain belt, suggesting the presence of denser material at depth or incomplete isostatic compensation. The
381 north-to-south younging of post-collisional volcanism (Seghedi et al., 2004) suggests that slab detachment
382 propagated southward over time, with the East Carpathians experiencing earlier break-off than the SE Carpathians.
383 If asthenospheric upwelling and lithospheric weakening occurred during that time, they could have led to
384 prolonged crustal adjustments that continue to manifest as uplift today.

385 In addition to the SE and East Carpathians, we also identify localized uplift in the South Carpathians. This region
386 marks the collision between the Dacia Block and the Moesian Platform, where oblique thrusting over the thick
387 Moesian lithosphere (Mañenco et al., 1997) may be inducing flexural or isostatic responses (Bertotti et al., 2003).
388 Bouguer gravity anomalies in this area transition from strongly negative values (~-100 mGal) near the foredeep
389 in the south to over +100 mGal at the contact with the Transylvanian Basin (Fig. 8), indicating a shift from thick,
390 low-density crust to denser material in the north. This pattern suggests differential isostatic compensation, where
391 northward crustal thinning leads to less mass deficit and reduced buoyancy, potentially causing flexural uplift.
392 This contrast could drive vertical displacements, as observed. Alternatively, deeper mantle processes, such as
393 residual slab dynamics or lithospheric-scale deformation associated with orogenic curvature, may also influence
394 the observed uplift.

395
396
397
398
399

400 **7. Conclusions**

401 This study integrates the most stable and longest GPS data records from Romania over a period of 20 years. Our
402 results provide a substantial improvement in spatial coverage and resolution of vertical and horizontal crustal
403 motions in a tectonically complex region sitting at the transition between dynamically active subduction systems
404 and the stable East European Platform, with additional influences exerted by a descending slab.

405 We observe pronounced horizontal southward motion in the Moesian Platform, minimal motion in the
406 Transylvanian Basin and East Carpathians, and a slight north-west motion of the Eastern European Platform, in a
407 Eurasian reference frame. The relative motions between these regions generate a dominantly extensional strain
408 field with localized zones of compression and shear, broadly consistent with stress regimes inverted from
409 earthquake clusters, although individual events capture more localized deformation heterogeneity.

410 Earlier studies in the region relied on campaign-style GPS observations. In contrast, our dataset includes cGPS
411 data from 130 stations spanning more than 20 years, providing improved spatial density and temporal resolution.
412 Our extended and more reliable data also reveal uplift in the foredeep of the SE Carpathians, challenging a
413 previously held view that this area is solely subsiding based on temporary GPS station data. This insight provides
414 a new perspective on the region's slab dynamics, which may be influenced by slab break-off and the fragmented
415 nature of the foreland, with its blocks of varying rheological strength. These differential vertical motions are
416 accommodated by seismically active faults on a crustal scale.

417 Overall, this study significantly advances our understanding of the tectonic processes that shape regions at the
418 intersection of active subduction/collision zones and stable continental platforms. It provides key constraints on
419 the interplay between slab dynamics, surface plate kinematics, and the resulting crustal deformation, an essential
420 step toward improving seismic hazard assessment.

421 **Code availability**

422 The GipsyX software is licensed to the Department of Geophysics of the University of Bucharest (UNIBUC). We
423 were allowed to use this software in an ongoing collaboration with UNIBUC. The strain rate estimation code
424 STRAINTOOL (Anastasiou et al., 2021) is available at <https://github.com/DSOlab/StrainTool> (accessed in
425 January 2025). Most figures were made using the open-source GMT software (Wessel et al., 2013).

426 **Data availability**

427 The RINEX-format GNSS data (sampled at 30s intervals) analyzed in this study are only available from the NIEP
428 (National Institute of Earth Physics) network online at <http://gps.infp.ro/#/>. The rest of the data can be made
429 available from the organisations responsible with their maintenance upon reasonable request and data sharing
430 agreements. All individual velocity solutions and strain rate estimates from this study are provided in the SM.

431

432

433 **Author contributions**

434 **AM:** Conceptualization, Methodology, Data Curation, Formal analysis, Investigation, Writing - Original Draft,
435 Visualization **LP:** Formal analysis, Writing - Original Draft, Visualization **BA:** Software, Data Curation, Formal
436 analysis, Visualization, Writing - Review & Editing, Supervision **FB:** Writing - Review & Editing **EN:** Writing -
437 Review & Editing, Managed the NIEP GNSS network technically **IM:** Writing - Review & Editing

438 **Competing interests**

439 The authors declare that they have no conflict of interest.

440 **Acknowledgments**

441 We acknowledge the Netherlands Research Centre for Integrated Solid Earth Science (ISES) for the initial
442 establishment in 2001 of seven cGPS stations in Romania dedicated to long term geodetic and geophysical
443 research in the region. This early enterprise comprised a collaborative effort of the University of Bucharest (V.
444 Mocanu), the National Institute for Earth Physics (L. Munteanu), the Delft University of Technology (B.A.C.
445 Ambrosius), and the Utrecht University (W. Spakman). We thank the National Research and Development
446 Institute for Marine Geology and Geo-Ecology, National Center for Monitoring and Alarm to Natural Marine
447 Hazards – Euxinus, as well as the National Agency for Cadaster and Land Registration, and the TopGeocart
448 company for providing access to their data. The authors thank Dr. Stefan Leinen, an anonymous reviewer, and the
449 editors for their constructive comments on the original manuscript.

450 **Financial support**

451 This research was carried out within the NUCLEU project, SOL4RISC Program which is supported by the
452 Ministry of Education and Research, project nr. PN23360201. This work was also supported by the European
453 Union (Next Generation EU instrument) through the National Recovery and Resilience Plan, "PNRR-III-C9-2022
454 – I5 Establishment and operationalization of Competence Centers" competition, "Competence Center for Climate
455 Change Digital Twin for Earth forecasts and societal redressment: DTEClimate" project, contract
456 no.760008/30.12.2022, code 7/16.11.2022. Additional support was provided through the CRESCENTO Project
457 (no. 346/390022/08.09.2021, SMIS no. 127463) and the GEOMONITOR Project (contract no. 28Sol(T28)/2025),
458 funded by the Ministry of Education and Research through UEFISCDI within PNCDI IV.

459 **References**

- 460 Altamimi, Z., Métivier, L., Rebischung, P., Rouby, H., and Collilieux, X.: ITRF2014 plate motion model,
461 Geophys. J. Int., 209, 1906–1912, <https://doi.org/10.1093/gji/ggx136>, 2017.
- 462 Anastasiou, D.G., Papanikolaou, X., Ganas, A., and Paradissis, D.: StrainTool: A software package to estimate
463 strain tensor parameters. Zenodo. Version 1.1, <https://doi.org/10.5281/zenodo.5501234>, 2021.

464 Amaru, M. L.: Global travel time tomography with 3-D reference models, PhD thesis, Utrecht Univ., Utrecht,
465 Netherlands, <http://hdl.handle.net/1874/19338>, 2007.

466 Andrews, E. R., and Billen, M. I.: Rheologic controls on the dynamics of slab detachment, *Tectonophysics*, 464,
467 60-69, <https://doi.org/10.1016/j.tecto.2007.09.004>, 2009.

468 Bada, G., Horváth, F., Dövényi, P., Szafián, P., Windhoffer, G., and Cloetingh, S.: Present-day stress field and
469 tectonic inversion in the Pannonian basin, *Global Planet. Change*, 58, 165-180,
470 <https://doi.org/10.1016/j.gloplacha.2007.01.007>, 2007.

471 Balla, Z.: Palaeotectonic reconstruction of the central Alpine-Mediterranean belt for the Neogene,
472 *Tectonophysics*, 127, 213-243, [https://doi.org/10.1016/0040-1951\(86\)90062-4](https://doi.org/10.1016/0040-1951(86)90062-4), 1986.

473 Bertiger, W., Bar-Sever, Y., Dorsey, A., Haines, B., Harvey, N., Hemberger, D., Heflin, M., Lu, W., Miller, M.,
474 Moore, A.W., Murphy, D., Ries, P., Romans, L., Sibois, A., Sibthorpe, A., Szilagy, B., Vallisneri, M., and Willis,
475 P.: GipsyX/RTGx, a new tool set for space geodetic operations and research, *Advances in Space Research*, 66,
476 469-489, <https://doi.org/10.1016/j.asr.2020.04.015>, 2020.

477 Bertotti, G., Maţenco, L., and Cloetingh, S. A. P. L.: Vertical movements in and around the south-east Carpathian
478 foredeep: lithospheric memory and stress field control. *Terra Nova*, 15, 299-305, 2003.

479 Beşuţiu, L., Manea, V., Pomeran, M.: Vrancea seismic zone as an unstable triple junction: new evidence from
480 observations and numerical modelling, in: *Proceedings of the 9th Congress of the Balkan Geophysical Society*,
481 *European Association of Geoscientists & Engineers*, 2017, 1-5, <https://doi.org/10.3997/2214-4609.201702541>,
482 2017.

483 Blewitt, G., Lavallée, D., Clarke, P., and Nurutdinov, K.: A new global mode of Earth deformation: Seasonal
484 cycle detected, *Science*, 294, 2.342-2.345, <https://doi.org/10.1126/science.106532001>, 2001.

485 Bonvalot, S., Balmirino, G., Briais, A., Kuhn, M., Peyrefitte, A., Vales, N., Biancale, R., Gabalda, G., Moreaux,
486 G., Reinquin, F., and Sarrailh, M.: *World Gravity Map, 1:50000000 map*, Eds.: BGI-CGMW-CNES-IRD, Paris,
487 2012.

488 Bos, M. S., and Scherneck, H. G.: Ocean tide loading provider, <http://holt.oso.chalmers.se/loading/index.html>,
489 2011.

490 Borleanu, F., Petrescu, L., Fojtikova, L., Munteanu, I., Silvennoinen, H., Placinta, A.O., Oros, E., and Enescu, B.:
491 ML 5.7 Southern Carpathians earthquake sequence: Insights from seismic observations, ESC2024-S17/50-808,
492 https://www.erasmus.gr/UsersFiles/microsite1277/Documents/ESC2024_Abstract_Book.pdf, 2024.

493 Cloetingh, S. A. P. L., Burov, E., Maţenco, L., Toussaint, G., Bertotti, G., Andriessen, P. A. M., Wortel, M. J. R.,
494 and Spakman, W.: Thermo-mechanical controls on the mode of continental collision in the SE Carpathians
495 (Romania), *Earth Planet. Sc. Lett.*, 218, 57-76, 2004.

496 Cloetingh, S., Bada, G., Maţenco, L., Lankreijer, A., Horváth, F., and Dinu, C.: Modes of basin (de) formation,
497 lithospheric strength and vertical motions in the Pannonian-Carpathian system: inferences from thermo-
498 mechanical modelling, *Geo. Soc. Mem.*, 32, 207-221, DOI: 10.1144/GSL.MEM.2006.032.01.12, 2006.

499 Cornea, I., Dragoescu, I., Popescu, M. N., and Visarion, M.: Monography of recent vertical crustal movements in
500 the S. R. of Romania (in Romanian), Preprint Central Inst. of Phys., 100, 1978.

501 Cornea, I., and Popescu, M. N.: The Vrancea Earthquake of March 4, 1977, and the Recent crustal vertical
502 movements in Romania. In Cornea & Radu (Editors): Seismological Research of March 4, 1977 Earthquake (in
503 Romanian), Preprint Central Inst. of Phys., 559 - 568, 1979a.

504 Cornea, I., Dragoescu, I., Popescu, M. N., and Visarion, M.: Map of recent vertical crustal movements of the
505 territory of S. R. of Romania (in Romanian), St. Cerc. Geol., Geofiz., Geogr., Geofizica, 17, 3-20, 1979b.

506 Craiu, A., Craiu, M., Diaconescu, M., and Marmureanu, A.: 2013 Seismic swarm recorded in Galati area,
507 Romania: focal mechanism solutions, Acta Geod. Geophys., 52, 53-67, 2017.

508 Csontos, L., and Vörös, A.: Mesozoic plate tectonic reconstruction of the Carpathian region, Palaeogeography,
509 Palaeoclimatology, Palaeoecology, 210, 1-56, <https://doi.org/10.1016/j.palaeo.2004.02.033>, 2004.

510 Dinter, G., and Schmitt, G.: Three Dimensional Plate Kinematics in Romania, Nat. Hazards, 23, 389–406,
511 <https://doi.org/10.1023/A:1011116615142>, 2001.

512 Duretz, T., Gerya, T. V., and May, D. A.: Numerical modelling of spontaneous slab breakoff and subsequent
513 topographic response, Tectonophysics, 502, 244-256, <https://doi.org/10.1016/j.tecto.2010.05.024>, 2011.

514 Enescu, B., Ghiță, C., Moldovan, I. A., and Radulian, M.: Revisiting Vrancea (Romania) intermediate-depth
515 seismicity: some statistical characteristics and seismic quiescence testing, Geosciences, 13, 219,
516 <https://doi.org/10.3390/geosciences13070219>, 2023.

517 Heidbach, O., Ledermann, P., Kurfeß, D., Peters, G., Buchmann, T., Mañenco, L., Negut, M., Sperner, B., Müller,
518 B., and Nuckelt, A.: Attached or not attached: slab dynamics beneath Vrancea, Romania, In: International
519 symposium on strong Vrancea earthquakes and risk mitigation, 4–20, 2007.

520 Heidbach, O., Rajabi, M., Cui, X., Fuchs, K., Müller, B., Reinecker, J., Reiter, K., Tingay, M., Wenzel, F., Xie,
521 F., and Ziegler, M.O.: The World Stress Map database release 2016: Crustal stress pattern across scales,
522 Tectonophysics, 744, 484-498, 2018.

523 Hippolyte, J. C.: Geodynamics of Dobrogea (Romania): new constraints on the evolution of the Tornquist–
524 Teisseyre Line, the Black Sea and the Carpathians, Tectonophysics, 357, 33-53, [https://doi/10.1016/S0040-
525 1951\(02\)00361-X](https://doi/10.1016/S0040-1951(02)00361-X), 2002.

526 Ismail-Zadeh, A., Mañenco, L., Radulian, M., Cloetingh, S., and Panza, G.: Geodynamics and intermediate-depth
527 seismicity in Vrancea (the south-eastern Carpathians): current state-of-the art. Tectonophysics, 530, 50-79, DOI:
528 10.1016/j.tecto.2012.01.016, 2012.

529 Joó, I., Arabadžijski, D., Fűry, M., Meščerski, I. N., Mihăila, M., Mladenovski, M. M., Németh, Z., Steinberg, J.,
530 Thury, J., Vanko, J., and Wyrzykowski, T.: New investigations or recent vertical movements in the Carpatho-
531 Balkan region, J. Geodyn., 8, 99-113, [https://doi.org/10.1016/0264-3707\(87\)90028-7](https://doi.org/10.1016/0264-3707(87)90028-7), 1987.

532 Koulakov, I., Zaharia, B., Enescu, B., Radulian, M., Popa, M., Parolai, S., and Zschau, J.: Delamination or slab
533 detachment beneath Vrancea? New arguments from local earthquake tomography, *Geochem. Geophys. Geosy.*,
534 11, Q03002, <https://doi.org/10.1029/2009GC002811>, 2010.

535 Krézsek, C., Lăpădat, A., Mațenco, L., Arnberger, K., Barbu, V., and Olaru, R.: Strain partitioning at orogenic
536 contacts during rotation, strike–slip and oblique convergence: Paleogene-Early Miocene evolution of the contact
537 between the South Carpathians and Moesia, *Global Planet. Change*, 103, 63–81, [https://doi.org/10.1016/j.gloplacha](https://doi.org/10.1016/j.gloplacha.2012.11.009)
538 2012.11.009, 2013.

539 Lorinczi, P., and Houseman, G.: Lithospheric gravitational instability beneath the Southeast Carpathians,
540 *Tectonophysics*, 474, 322–336, <https://doi.org/10.1016/j.tecto.2008.05.024>, 2009.

541 Mațenco, L., Zoetemeijer, R., Cloetingh, S., and Dinu, C.: Lateral variations in mechanical properties of the
542 Romanian external Carpathians: inferences of flexure and gravity modelling, *Tectonophysics*, 282,147-166,
543 [https://doi.org/10.1016/S0040-1951\(97\)00217-5](https://doi.org/10.1016/S0040-1951(97)00217-5), 1997.

544 Mațenco, L., and Bertotti, G.: Tertiary tectonic evolution of the external East Carpathians (Romania),
545 *Tectonophysics*, 316, 255–286, [https://doi.org/10.1016/S0040-1951\(99\)00261-9](https://doi.org/10.1016/S0040-1951(99)00261-9), 2000.

546 Mațenco, L., Bertotti, G., Cloetingh, S., and Dinu, C.: Subsidence analysis and tectonic evolution of the external
547 Carpathian-Moesian platform region during Neogene times, *Sed Geol*, 156, 71-94, [https://doi.org/10.1016/S0037-](https://doi.org/10.1016/S0037-0738(02)00283-X)
548 0738(02)00283-X, 2003.

549 Mațenco, L., Bertotti, G., Leever, K., Cloetingh, S.A.P.L., Schmid, S.M., Tărăpoancă, M., and Dinu, C.: Large-
550 scale deformation in a locked collisional boundary: Interplay between subsidence and uplift, intraplate stress, and
551 inherited lithospheric structure in the late stage of the SE Carpathians evolution, *Tectonics*, 26, TC4011,
552 <https://doi.org/10.1029/2006TC001951>, 2007.

553 Mațenco, L. and Radivojević, D.: On the formation and evolution of the Pannonian Basin: Constraints derived
554 from the structure of the junction area between the Carpathians and Dinarides, *Tectonics*, 31, TC6007,
555 <https://doi.org/10.1029/2012TC003206>, 2012.

556 Merten, S., Andriessen, P. A. M., Juez-Larré, J., Bertotti, G. V., and Dunai, T. J.: Dating the exhumation of the
557 Romanian Carpathians: first results from apatite (U-Th)/He thermochronology, *Abstract from Geophysical*
558 *Research Abstracts*, 7, 08138, [https://meetings.copernicus.org/www.cosis.net/abstracts/EGU05/08138/EGU05-J-](https://meetings.copernicus.org/www.cosis.net/abstracts/EGU05/08138/EGU05-J-08138.pdf)
559 08138.pdf, 2005.

560 Merten, S., Mațenco, L., Foeken, J. P. T., Stuart, F. M., and Andriessen P. A. M.: From nappe stacking to out-of-
561 sequence postcollisional deformations: Cretaceous to Quaternary exhumation history of the SE Carpathians
562 assessed by low-temperature thermochronology, *Tectonics*, 29, TC3013, <https://doi.org/10.1029/2009TC002550>,
563 2010.

564 Müller, B., Heidbach, O., Negut, M., Sperner, B. and Buchmann, T.: Attached or not attached—evidence from
565 crustal stress observations for a weak coupling of the Vrancea slab in Romania, *Tectonophysics*, 482, 139-149,
566 <https://doi.org/10.1016/j.tecto.2009.08.022>, 2010.

- 567 Muntean, A., Mocanu, V., Ambrosius, B.: A GPS study of land subsidence in the Petrosani (Romania) coal
568 mining area. *Nat. Hazards*, 80, 797–810, DOI:10.1007/s11069-015-1997-y, 2016.
- 569 Necea, D., Fielitz, W., and Maţenco, L.: Late Pliocene–Quaternary tectonics in the frontal part of the SE
570 Carpathians: Insights from tectonic geomorphology, *Tectonophysics*, 410, 137-156,
571 <https://doi.org/10.1016/j.tecto.2005.05.047>, 2005.
- 572 Necea, D., Fielitz, W., Kadereit, A., Andriessen, P. A. M., and Dinu, C.: Middle Pleistocene to Holocene fluvial
573 terrace development and uplift-driven valley incision in the SE Carpathians, Romania, *Tectonophysics*, 602, 332-
574 354, <https://doi.org/10.1016/j.tecto.2013.02.039>, 2013.
- 575 Necea, D., Juez-Larré, J., Maţenco, L., Andriessen, P. A. M., and Dinu, C.: Foreland migration of orogenic
576 exhumation during nappe stacking: Inferences from a high-resolution thermochronological profile over the
577 Southeast Carpathians, *Global Planet. Change*, 200, 103457, <https://doi.org/10.1016/j.gloplacha.2021.103457>,
578 2021.
- 579 Nemcok, M., Pospisil, L., Lexa, J., and Donelick, R.A.: Tertiary subduction and slab break-off model of the
580 Carpathian–Pannonian region, *Tectonophysics*, 295, 307-340, [https://doi.org/10.1016/S0040-1951\(98\)00092-4](https://doi.org/10.1016/S0040-1951(98)00092-4),
581 1998.
- 582 Petrescu, L., Stuart, G., Tătaru, D., and Grecu, B.: Crustal structure of the Carpathian Orogen in Romania from
583 receiver functions and ambient noise tomography: how craton collision, subduction and detachment affect the
584 crust. *Geophys. J. Int.*, 218, 163-178, <https://doi.org/10.1093/gji/ggz140>, 2019.
- 585 Petrescu, L., Borleanu, F., Radulian, M., Ismail-Zadeh, A., and Maţenco, L.: Tectonic regimes and stress patterns
586 in the Vrancea Seismic Zone: Insights into intermediate-depth earthquake nests in locked collisional settings,
587 *Tectonophysics*, 799, 228688, <https://doi.org/10.1016/j.tecto.2020.228688>, 2021.
- 588 Petrescu, L., Mihai, A., and Borleanu, F.: Slab tear and rotation imaged with core-refracted shear wave anisotropy,
589 *J. Geodyn.*, 157, 101985, <https://doi.org/10.1016/j.jog.2023.101985>, 2023.
- 590 Petrescu, L. and Enescu, B.: Seismicity of a relic slab: space–time cluster analysis in the Vrancea Seismic Zone,
591 *Earth, Planets and Space*, 77, 6., <https://doi.org/10.1186/s40623-025-02136-6>, 2025.
- 592 Piña-Valdés, J., Socquet, A., Beauval, C., Doin, M.-P., D’Agostino, N., and Shen, Z.-K.: 3D GNSS velocity field
593 sheds light on the deformation mechanisms in Europe: Effects of the vertical crustal motion on the distribution of
594 seismicity, *J. Geophys. Res.-Sol. Ea.*, 127, e2021JB023451, <https://doi.org/10.1029/2021JB023451>, 2022.
- 595 Poncoş, V., Stanciu, I., Teleagă, D., Maţenco, L., Bozsó, I., Szakács, A., Birtas, D., Toma, S.A., Stănică, A.,
596 and Rădulescu, V.: An Integrated Platform for Ground-Motion Mapping, Local to Regional Scale; Examples from
597 SE Europe, *Remote Sensing*, 14, 1046, 10.3390/rs14041046, 2022.
- 598 Popa, M., Chircea, A., Dinescu, R., Neagoe, C., Grecu, B., and Borleanu, F.: Romanian earthquake catalogue
599 (ROMPLUS), *Mendeley Data*, 2, 2022.
- 600 Popescu, M. N., and Drăgoescu, I.: Maps of recent vertical crustal movements in Romania: Similarities and
601 differences, *J. Geodyn.*, 8, 123-136, [https://doi.org/10.1016/0264-3707\(87\)90030-5](https://doi.org/10.1016/0264-3707(87)90030-5), 1987.

602 Radulian, M., Bălă, A., Ardeleanu, L., Toma-Dănilă, D., Petrescu, L., and Popescu, E.: Revised catalogue of
603 earthquake mechanisms for the events occurred in Romania until the end of twentieth century: REFMC, *Acta*
604 *Geod. Geophys.*, 54, 3-18, <https://doi.org/10.1007/s40328-018-0243-y>, 2019.

605 Radulian, M., Popa, M., Dinescu, R., and Bălă, A.: Location improvements for the twin crustal earthquakes
606 recorded in February 2023 in Gorj County, Romania, *International Multidisciplinary Scientific GeoConference:*
607 *SGEM*, 23(1.1), 57-64, 2023.

608 Ren, Y., Stuart, G., Houseman, G., Dando, B., Ionescu, C., Hegedüs, E., Radovanović, S., and Shen, Y.: Upper
609 mantle structures beneath the Carpathian–Pannonian region: Implications for the geodynamics of continental
610 collision, *Earth Planet. Sc. Lett.*, 349, 139–152. <https://doi.org/10.1016/j.epsl.2012.06.037>, 2012.

611 re3data.org: VMF Data Server; editing status 2024-05-15; re3data.org - Registry of Research Data Repositories,
612 <https://doi.org/10.17616/R3RD2H>

613 Sanders, C., Andriessen, P., and Cloetingh, S.: Life cycle of the East Carpathian orogen: erosion history of a
614 doubly vergent critical wedge assessed by fission track thermochronology, *J. Geophys. Res.*, 104, 29095–29112,
615 <https://doi.org/10.1029/1998JB900046>, 1999.

616 Săndulescu, M.: *Geotectonica României*. Ed. Tehnică, București, 336 pp. 1984.

617 Schmid, S. M., Fügenschuh, B., Kounov, A., Mařenco, L., Nievergelt, P., Oberhänsli, R., Pleuger, J., Schefer, S.,
618 Schuster, R., Tomljenović, B., and Ustaszewski, K.: Tectonic units of the Alpine collision zone between Eastern
619 Alps and western Turkey, *Gondwana Res.*, 78, 308-374, <https://doi.org/10.1016/j.gr.2019.07.005>, 2020.

620 Seghedi, A., Lang, B., and Heimann, A.: The deformational history of North Dobrogean Hercynian basement as
621 reflected in new ³⁹Ar/⁴⁰Ar determinations, *Romanian Journal of Tectonics and Regional Geology*, 77, 64-65,
622 <https://doi.org/10.3906/YER-1101-20>, 1999.

623 Seghedi, I., Downes, H., Vaselli, O., Szakács, A., Balogh, K. and Pécskay, Z.: Post-collisional Tertiary–
624 Quaternary mafic alkalic magmatism in the Carpathian–Pannonian region: a review, *Tectonophysics*, 393, 43-62,
625 <https://doi.org/10.1016/j.tecto.2004.07.051>, 2004.

626 Serpelloni, E., Cavaliere, A., Martelli, L., Pintori, F., Anderlini, L., Borghi, A., Randazzo, D., Bruni, S., Devoti,
627 R., Perfetti, P., and Cacciaguerra, S.: Surface Velocities and Strain-Rates in the Euro-Mediterranean Region From
628 Massive GPS Data Processing, *Front. Earth Sci.*, 10, 907897, <https://doi.org/10.3389/feart.2022.907897>, 2022.

629 Shen, Z. K., Wang, M., Zeng, Y., and Wang, F.: Strain determination using spatially discrete geodetic data, *Bull.*
630 *Seismol. Soc. Am.*, 105, 2117-2127, <https://doi.org/10.1785/0120140247>, 2015.

631 Sperner, B.: Computer programs for the kinematic analysis of brittle deformation structures and the Tertiary
632 tectonic evolution of the Western Carpathians. *Tübingen Geoscientific Works (TGA) Series A. Geology,*
633 *Paleontology, Stratigraphy* 27 (NEBIS)001536648EBI01, 1996.

634 Sperner, B., Lorenz, F., Bonjer, K., Hettel, S., Müller, B., and Wenzel, F: Slab break-off–abrupt cut or gradual
635 detachment? New insights from the Vrancea Region (SE Carpathians, Romania), *Terra Nova*, 13, 172-179,
636 <https://doi.org/10.1046/j.1365-3121.2001.00335.x>, 2001.

637 Tărăpoancă, M., Garcia-Castellanos, D., Bertotti, G., Mațenco, L., Cloetingh, S., and Dinu, C.: Role of the 3-D
638 distributions of load and lithospheric strength in orogenic arcs: polystage subsidence in the Carpathians foredeep,
639 *Earth Planet. Sc. Lett.*, 221, 163–180, [https://doi.org/10.1016/S0012-821X\(04\)00068-8](https://doi.org/10.1016/S0012-821X(04)00068-8), 2004.

640 Van der Hoeven, A., Mocanu, V., Spakman, W., Nutto, M., Nuckelt, A., Mațenco, L., Munteanu, L., Marcu, C.,
641 and Ambrosius, B.: Observation of present-day tectonic motions in the Southeastern Carpathians: Results of the
642 ISES/CRC-461 GPS measurements, *Earth Planet. Sc. Lett.*, 239, 177-
643 184, <https://doi.org/10.1016/j.epsl.2005.09.018>, 2005.

644 Wenzel, F., Lorenz, F., Sperner, B., and Oncescu, M. C.: *Seismotectonics of the Romanian Vrancea area, Vrancea*
645 *Earthquakes: Tectonics, Hazard and Risk Mitigation*, 15–26, Kluwer Acad., 1999.

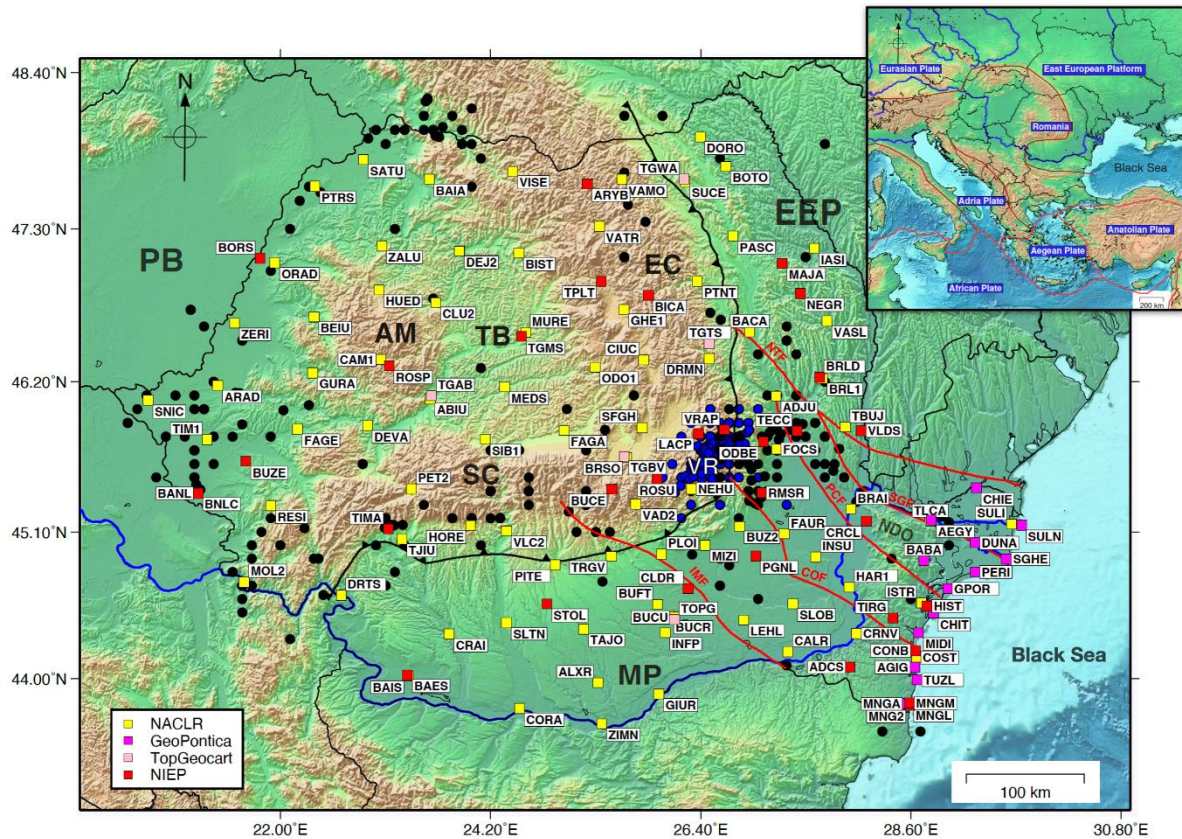
646 Wessel, P., W. H. Smith, R. Scharroo, J. Luis, and F. Wobbe: *Generic Mapping Tools: Improved Version*
647 *Released*, *Eos, Trans. AGU*, 94, 409–410, <https://doi.org/10.1002/2013EO450001>, 2013.

648 Wortel, M. J. R., and Spakman, W.: Subduction and slab detachment in the Mediterranean-Carpathian region,
649 *Science*, 290, 1910-1917, [https://doi.org/DOI: 10.1126/science290.5498.1910](https://doi.org/DOI:10.1126/science290.5498.1910), 2000.

650
651
652
653
654
655
656
657
658
659
660
661
662
663
664
665
666
667
668
669
670

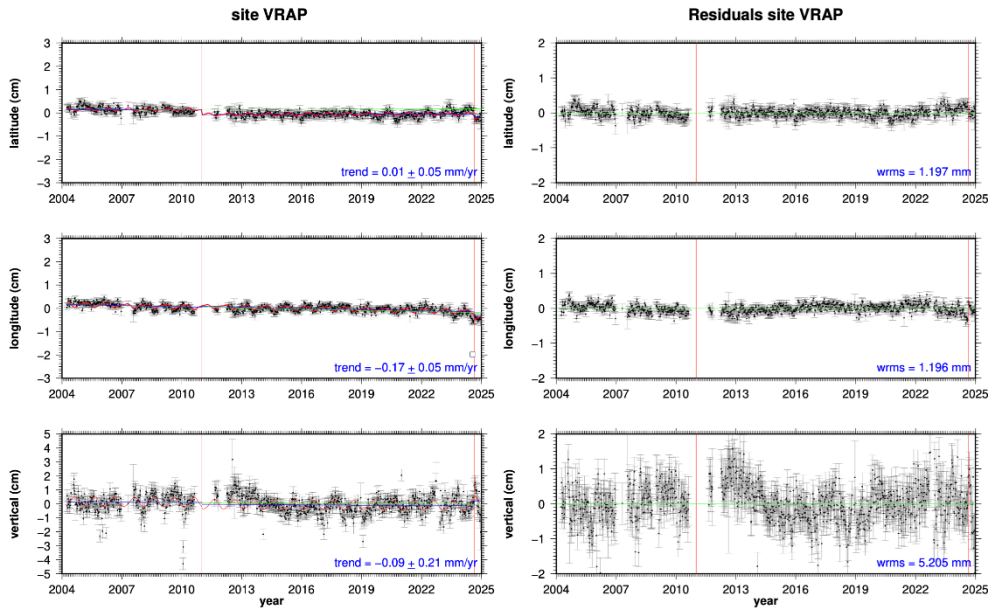
671 Figures

672



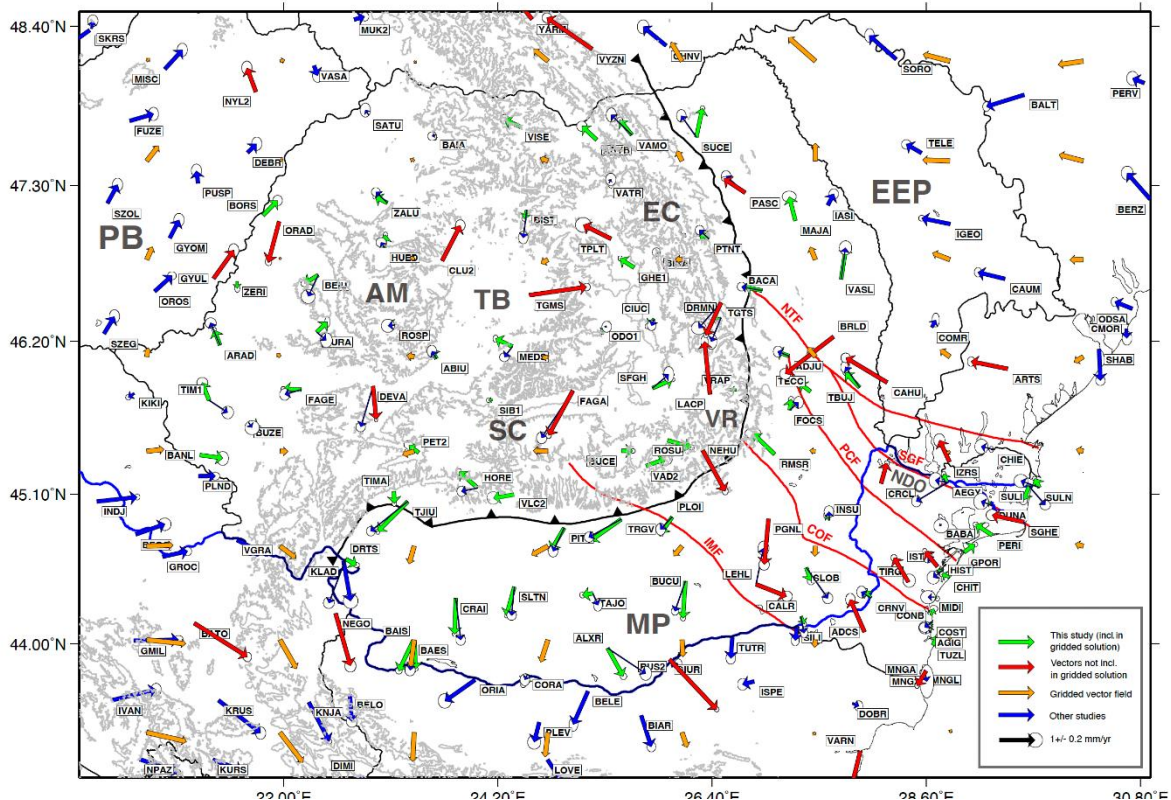
673

674 Figure 1: The distribution of the available cGPS stations used in this study (coloured squares), and earthquakes
675 distribution according to the Romanian earthquakes catalog (ROMPLUS, Popa et al., 2022) between August 1679 and
676 September 2024. Earthquakes are color-coded by depth: black for crustal events ($H < 60$ km, $M_w > 3.5$), blue for
677 intermediate-depth events ($60 < H$ (km) < 167 , $M_w > 4$). The major faults are plotted as solid red lines and identified
678 with their acronyms: IMF - Intra-Moesian Fault, COF - Capidava Ovidiu Fault, PCF - Peceneaga Camena Fault, NTF
679 - New Trotuș Fault, and SGF - Sfântu Gheorghe Fault. The old trust fault is represented by a solid, black, toothed line.
680 The major tectonic units are in bold characters: AM - Apuseni Mountains, SC - South Carpathians, EC - East
681 Carpathians, VR - Vrancea, NDO - North Dobrogea Orogen, PB - Pannonian Basin, TB - Transylvanian Basin, EEP -
682 East European Platform, and MP - Moesian Platform. Further acronyms in the color legend box include: NACL -
683 National Agency for Cadastre and Land Registration, GeoPontica - National Research-Development Institute for
684 Marine Geology and Geocology GNSS network, TopGeocart is a private company, operating its own GNSS network,
685 NIEP - National Institute for Earth Physics. The inset shows the regional tectonic setting, with plate boundaries
686 indicated in red.



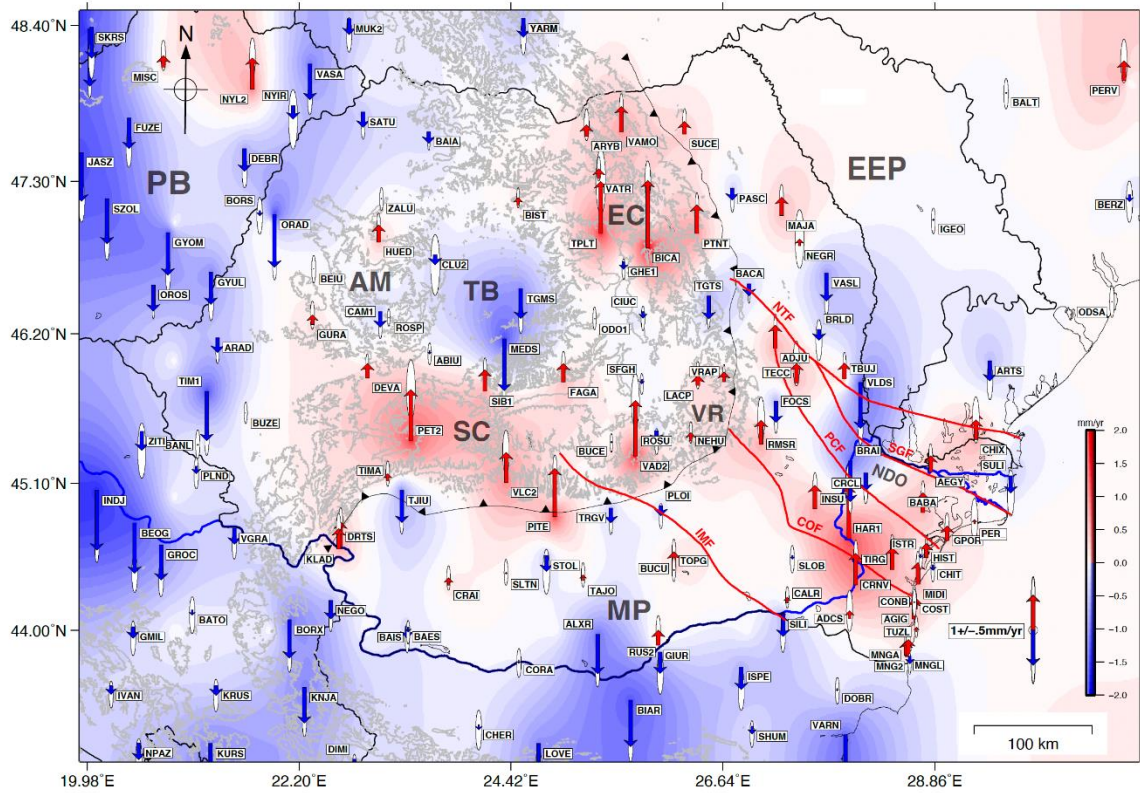
687
688
689
690
691

Figure 2: Time series of the VRAP station. The left panel shows the raw series with the modeled functions. The red curve represents the estimated yearly and half-yearly functions. In the left panel, the green line represents the estimated velocity before the first jump. The vertical red lines represent position jumps. The right panel shows the residuals after subtracting the modeled functions, including the estimated position jumps.



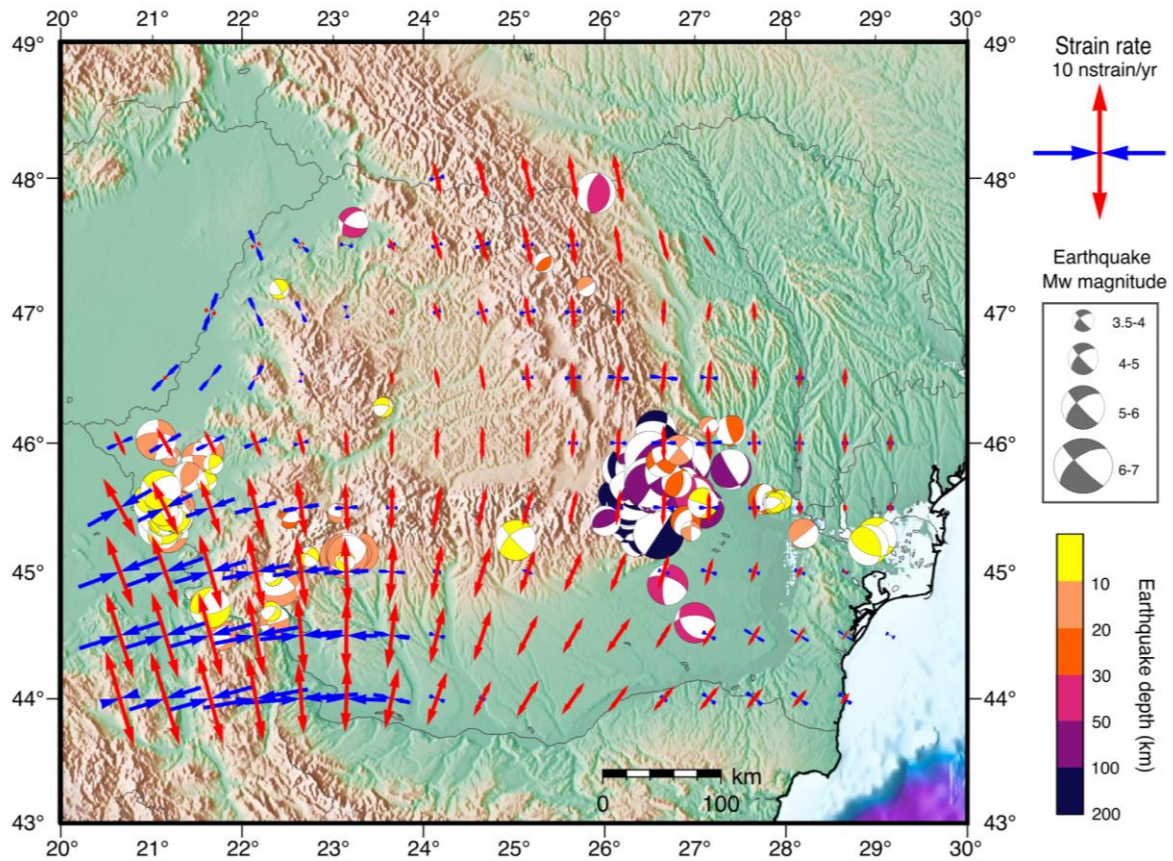
692
693
694
695
696
697

Figure 3: GPS-derived horizontal velocity vectors with respect to the ITRF-2014 Eurasian plate according to Altamimi et al. (2017). Green vectors represent our results, blue vectors were taken from Piña-Valdés et al. (2022). The red vectors were excluded while creating the interpolated velocity field on a regular (8 x 8) grid, represented as orange vectors. The error ellipses are 95% confidence level. Faults and acronyms are as in Figure 1.



698

699 **Figure 4: GPS-derived vertical velocity vectors. Red vectors indicate uplift, while blue vectors indicate subsidence. The**
 700 **background is a gridded interpolation field. The error ellipses are at the 95% confidence level. Faults and acronyms**
 701 **are as in Figure 1.**

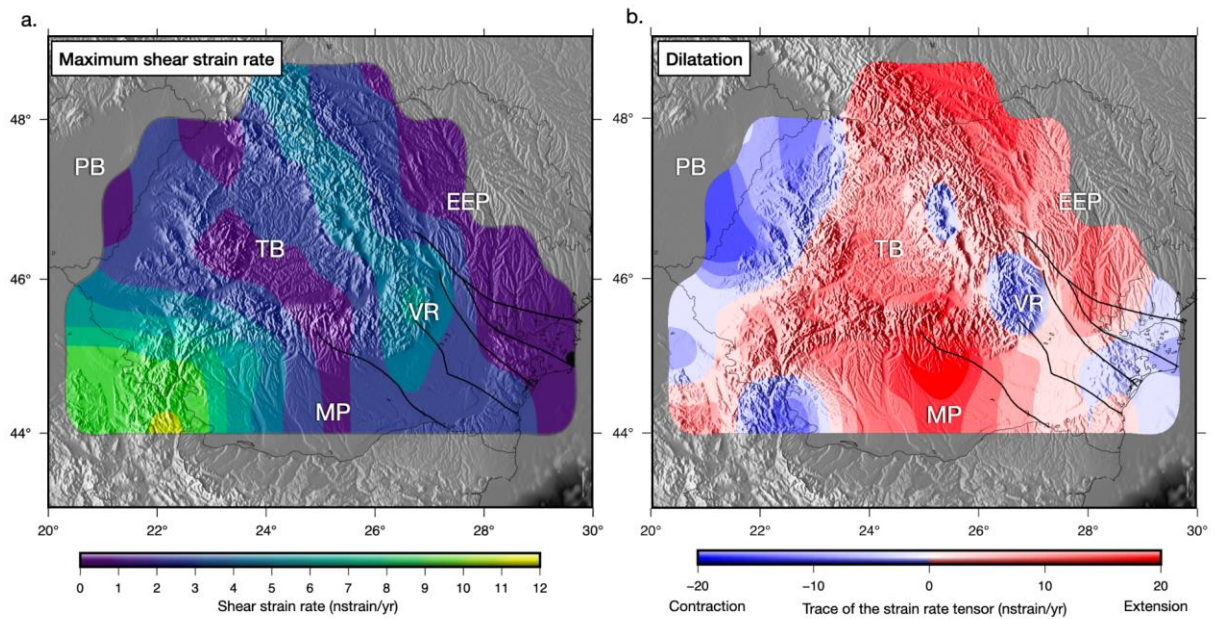


702

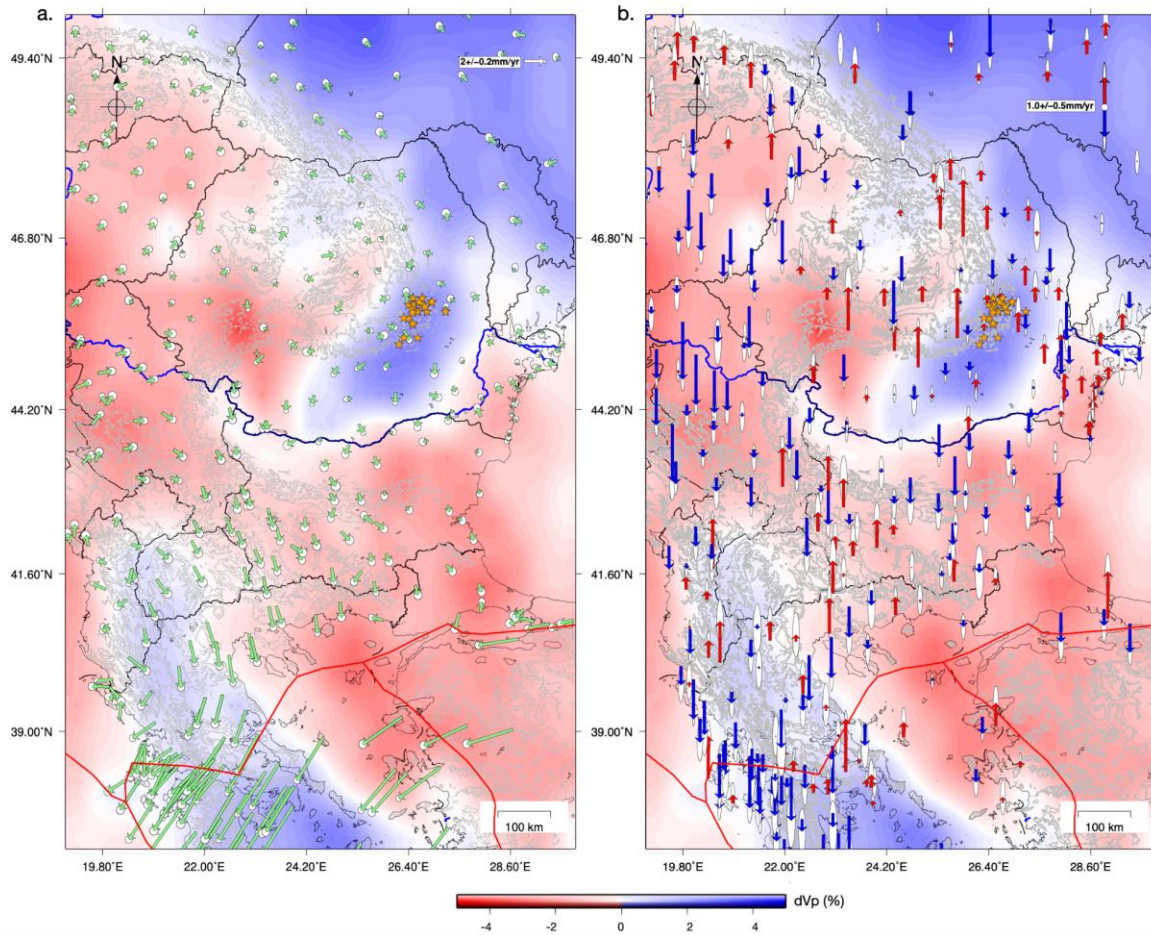
703 **Figure 5: Map showing the principal axes of strain rates determined from the regularized GPS horizontal velocity**
 704 **vector field from this study and mechanisms of earthquakes with $M_w > 3.5$ from the REFMC catalogue (Radulian et**
 705 **al., 2019).**

706

707



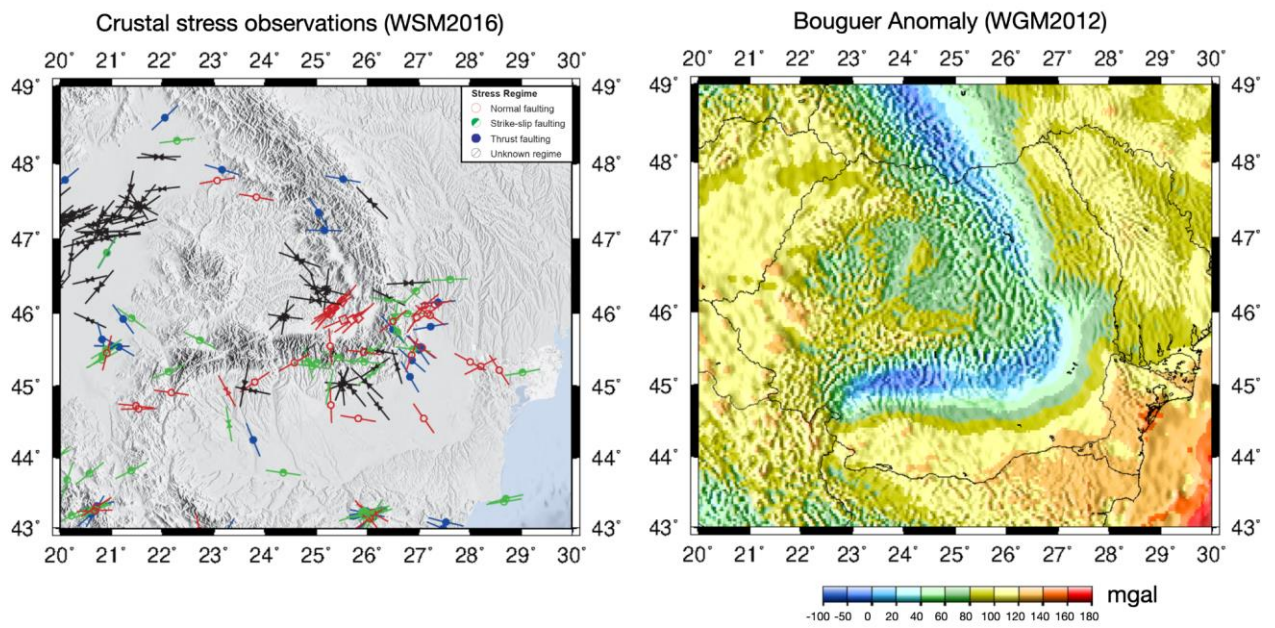
709 **Figure 6:** Maps showing (a) maximum shear strain rate and (b) dilatational strain rate (both in nanostrain/year),
 710 derived from the regularized GPS velocity field in Romania (Table S2, SM). The maximum shear strain rate illustrates
 711 the intensity and direction of lateral crustal deformation, while the dilatational strain rate is the trace of the strain rate
 712 tensor (volumetric rate of change) and indicates regions of extension (red-positive) and compression (blue-negative).
 713 Major faults are shown as thick black lines. Acronyms are described in the caption of Figure 1.



714

715 **Figure 7: Regional horizontal (a) and vertical crustal motions (b) from this study, Serpelloni et al. (2022), and Piña-**
 716 **Valdés et al. (2022). The horizontal vector field was scaled for visibility. The background colours show Vp seismic**
 717 **velocity anomalies at 200 km depth from the UU-P07 seismic model of Amaru et al. (2007). Red lines mark the active**
 718 **plate boundaries between Eurasia, Anatolia, and Aegean plates in the south. Orange stars mark earthquakes $M_w > 6$**
 719 **from the Vrancea Zone (Radulian et al., 2019).**

720



722 **Figure 8: Left: Crustal stress observations compiled from focal mechanisms, borehole breakouts, and other geological**
 723 **indicators, from the World Stress Map (Heidbach et al., 2018). Colours indicate the most likely stress regime. Right:**
 724 **Bouguer gravity anomalies from the World Gravity Map (WGM2012) maintained by the Bureau Gravimétrique**
 725 **International (Bonvalot et al., 2012).**